Correspondence to:

S. Okumura,
satoshi.okumura.d2@tohoku.ac.jp

A Molecular-Scale Origin of Shear Thinning and Brittle Failure of Silicate Melt

S. Okumura[1] , **K. Uesugi[2]** , **A. Goto[3], K. Matsumoto[1], and T. Sakamaki[1]**

[1]Division of Earth and Planetary Materials Science, Department of Earth Science, Graduate School of Science, Tohoku University, Sendai, Japan, [2]SPring-8/Japan Synchrotron Radiation Research Institute, Sayo, Japan, [3]Center for Northeast Asian Studies, Tohoku University, Sendai, Japan

Abstract Shear thinning and brittle failure of silicate melt control the dynamics of volcanic eruptions, but their molecular-scale origin is still unclear. Here, we conducted tension and compression experiments on silicate melts, using time-resolved X-ray diffraction. Our experiments revealed that the intermediate-range ordering of silicate structures, that is, the ring size formed by the SiO_4 tetrahedra, demonstrated elastic and anisotropic dilation under tension and shrinkage under compression in the non-Newtonian regime. In contrast, there were no significant changes in short-range ordering, such as Si–O and Si–Si distances. Based on these findings, we inferred that shear thinning observed under high stress originates from the formation of anisotropically deformed large and small rings in silicate structures that are energetically unfavorable and unstable. Brittle failure occurred under high-stress conditions, in both tension and compression. We propose a stress criterion as a necessary and sufficient condition for magma failure, rather than a strain rate criterion.

Plain Language Summary Explosive volcanic eruptions occur when magma fragments and volcanic gases are released to the surface. However, magma is originally a continuous fluid that behaves like a liquid in the crust. To understand how magma fails during volcanic eruptions, we need to uncover the underlying mechanisms. This challenge was identified over four decades ago, and researchers proposed conducting molecular-scale experiments on magma deformation to shed light on its complex behavior, including brittle failure. However, this has been difficult to achieve experimentally. In this study, we used powerful X-ray sources at SPring-8 in Japan to address this challenge. Our findings reveal that the complex behavior of magma originates from previously unrecognized molecular-scale elastic and anisotropic deformation. Finally, we propose a criterion for magma failure that can help determine whether an eruption will be explosive.

1. Introduction

The rheological behavior of magma controls magma flow in the conduit and eruption dynamics. Brittle failure of the magma has a significant impact on dynamics as it changes the flow type from bubbly flow to gas-ash dispersion flow in the conduit (e.g., Kozono & Koyaguchi, 2012; Kozono & Okumura, 2022; Papale, 1999; Wilson et al., 1980). The brittle failure of magma originates from the failure of the supercooled silicate melt under high deformation rates; such a melt also exhibits shear-thinning behavior (Goto, 1999; Okumura et al., 2020; Simmons et al., 1982; Wadsworth et al., 2018; Webb and Dingwell, 1990a, 1990b). Additionally, the shear-thinning behavior of crystal-bearing magma (e.g., Caricchi et al., 2007; Champallier et al., 2008; Okumura et al., 2016) may originate from the rheology of the melt between the crystals (Vasseur et al., 2023). Therefore, it is essential to understand the mechanism of the non-Newtonian behavior of supercooled silicate melts for modeling volcanic eruptions and predicting their explosivity and style.

The molecular-scale origin of shear thinning and brittle failure in silicate melts remains unknown. This is mainly due to the experimental difficulties in investigating the molecular-scale properties of silicate melts under deformation, despite its importance, as highlighted by Simmons et al. (1982) in their pioneering study on the non-Newtonian behavior of supercooled silicate melts. However, recent advancements in strong X-ray sources have enabled time-resolved X-ray diffraction (XRD) and scattering experiments to investigate the molecular-scale structure of silicate melts under deformation (e.g., Di Genova et al., 2020; Okumura et al., 2020, 2022, 2023). Okumura et al. (2023) demonstrated, for the first time, that the molecular-scale structure of supercooled silicate melts elastically dilates in the direction of tension when the applied stress is high, that is, in the non-Newtonian
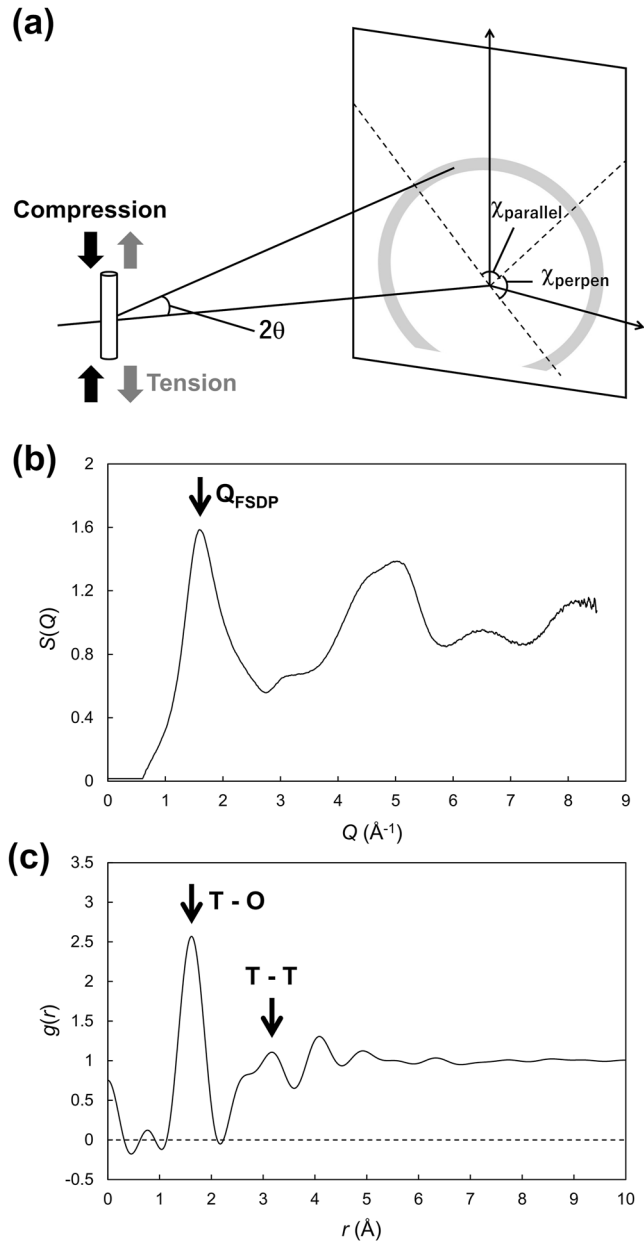
Figure 1. (a) Schematic drawing of the experimental setup, and the (b) structural factor $S(Q)$ and (c) radial distribution function $g(r)$ of rhyodacite melt at 840°C, obtained from an experiment with a tension rate of 20 μm s^{-1}. In (a) and (b), Q is defined as $4\pi \cdot \sin\theta/\lambda$, where θ and λ are half of the diffraction angle and wavelength, respectively. The peak positions of Q_{FSDP}, T–O, and T–T were determined by fitting the Gaussian curve.

regime. Molecular dynamics simulations of the tensile deformation of SiO$_2$ glass showed the formation of large rings composed of SiO$_4$ tetrahedra and a decrease in the number of medium-sized rings (Bamer et al., 2019). Therefore, the experimentally observed dilation of the silicate melt may involve an increase in the average size of the ring. This change in ring size is also expected to reduce the viscosity because large rings with high energy are unfavorable, unstable in silicate structures (Rino et al., 1993), and mechanically weak (Muralidharan et al., 2007). Based on these observations, it has been inferred that the elastic dilation of the silicate melt may cause a reduction in viscosity and lead to macroscopic failure through cavitation (Chen et al., 2007; Guan et al., 2013; Okumura et al., 2023; Sun & Wang, 2015; Yuan & Huang, 2014).

Silicate melts can exhibit shear thinning and brittle failure under compression, in addition to tensile deformation (e.g., Hess et al., 2007, 2008; Wadsworth et al., 2018). If the mechanisms behind shear thinning and brittle failure are the same under tension and compression, we would expect to find the formation of large rings during compression. However, isostatic compression experiments have shown the opposite, with a decrease in ring size at high pressures (e.g., Williams & Jeanloz, 1988). In this study, we conducted tension and compression experiments on silicate melts and used time-resolved XRD to investigate the evolution of intermediate- and short-range ordering. Based on our experimental results, we discuss the molecular-scale origin of shear thinning and brittle failure in silicate melts.

2. Materials and Methods

We performed tension and compression experiments at BL47XU of SPring-8 (Japan) following the experimental methods reported by Okumura et al. (2023) (Figure 1a). The starting materials for the experiments were glass fibers with a rhyodacite composition. For the tension experiments, two glass beads were attached to both ends of the fiber (0.617 and 0.807 mm in diameter and 22.13 and 20.96 mm long for elongation rates of 10 and 20 μm s^{-1}, respectively). The fiber was fixed between the upper and lower pistons using the beads and then heated and elongated in the furnace. For the compression experiments, fat fibers (1.213 and 1.223 mm in diameter and 10.18 and 9.96 mm long for compression rates of 20 and 50 μm s^{-1}, respectively) were sandwiched using the upper and lower pistons with flat surfaces, which are different pistons from those used in the tension experiments. Then, the fibers were compressed in a furnace. In our experiments, the compressed sample failed, as described in the following section, although it exhibited buckling deformation under slow deformation rates. All experiments were conducted at a temperature of 840°C; the elongation and compression rates reported in this study were 10 and 20 and 20 and 50 μm s^{-1}, respectively. At the experimental temperature, the viscosity of the rhyodacite melt was measured to be 7.40×10^{10} Pa s (Okumura et al., 2023). Under our experimental conditions, the sample showed non-Newtonian behavior, as reported in previous studies, that is, Weissenberg number $> \sim 0.001$ (e.g., Simmons et al., 1982; Wadsworth et al., 2018).

Time-resolved XRD was collected during tension and compression experiments using a flat panel (C10901D-40, Hamamatsu Photonics KK) every 100 ms (Figure 1a). In this study, we used the X-ray with an energy of 30 keV and a beam size of 200 × 200 μm. The beam position and distance between the sample and detector were calibrated based on CeO$_2$ analyses. Two-dimensional XRD was integrated along the directions parallel and perpendicular to the tension and compression directions, respectively, with an azimuth angle of 90° ($\chi_{parallel}$ and χ_{perpen}
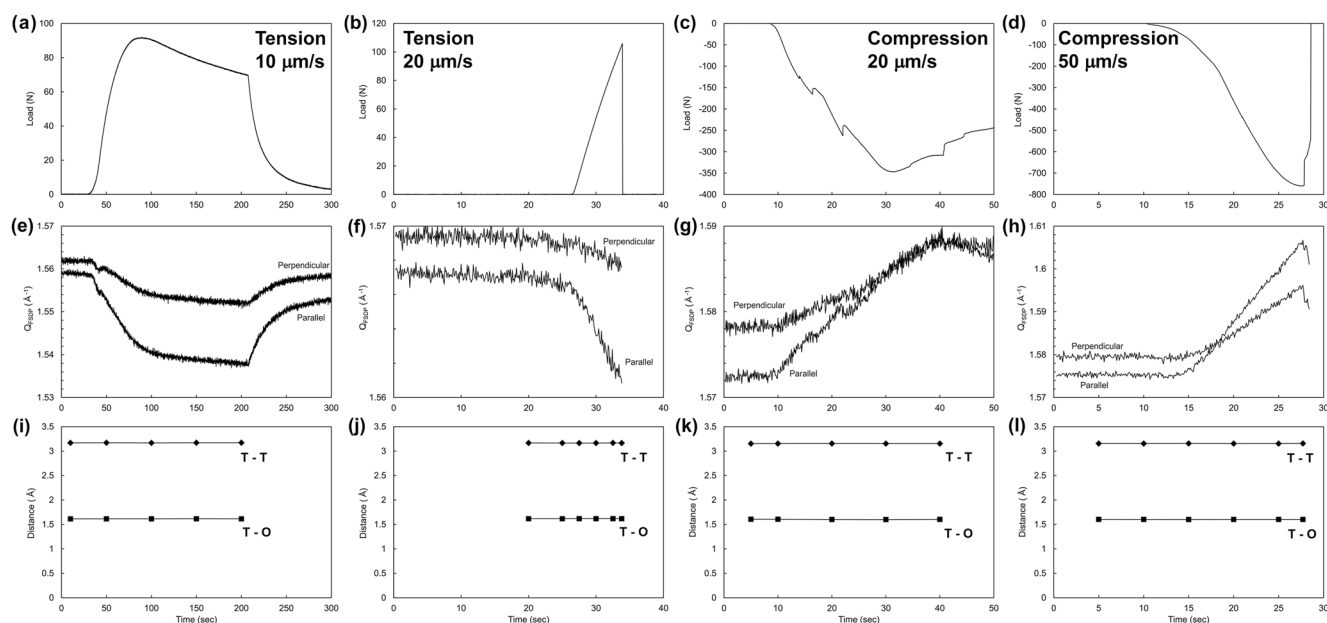
Figure 2. (a–d) Loads necessary for tension and compression, (e–h) Q_{FSDP} for parallel and perpendicular directions to tension and compression, and (i–l) T–O and T–T distances as functions of time. The rates of tension and compression are (a), (e), (i) 10, (b), (f), (j) 20, (c), (g), (k), 20, and (d), (h), (l) 50 μm s^{-1}, respectively. For all runs, the degree of change in Q_{FSDP} is larger in the direction parallel to the deformation, and no clear changes are observed in the T–O and T–T distances.

in Figure 1a). After integration, the position of the first sharp diffraction peak was determined by fitting it to a Gaussian curve (Q_{FSDP}). Then, the structural factor $S(Q)$ and radial distribution function $g(r)$ were calculated from typical XRD data obtained during tension and compression (Figures 1b and 1c). For the calculation of $S(Q)$ and $g(r)$, we used the Python-based software (Amorpheus) developed by Boccato et al. (2022). Because the 2θ angle was too small to calculate $g(r)$ for the direction perpendicular to the deformation, the calculation was performed only for the data parallel to the deformation. An atomic density of 70.2 (at/nm^3) was used in the calculation, which was estimated based on the melt density (2.38 g/cm^3) and average atomic weight (20.41 g/mol). The melt density was calculated at an experimental temperature of 840°C using the model of Lange and Carmichael (1990). The chemical composition of the melt was set as follows: O = 0.64, Si = 0.25, Al = 0.06, Na = 0.03, Mg = 0.01, and Ca = 0.01 (Okumura et al., 2023). The T–O and T–T distances, where T and O represent the T site cations (Si and Al) and oxygen, respectively, were obtained by fitting the Gaussian curve to the peaks in $g(r)$.

3. Experimental Results

3.1. Tension Experiments

The load needed to elongate the sample, Q_{FSDP}, and the T–O and T–T distances are summarized in Figure 2 as a function of time. Before heating the sample, small spaces were set between the sample and pistons to prevent failure during the heating; thus, there are small waiting periods before the load starts to increase. When the elongation rate was 10 μm s^{-1}, the load gradually increased in the first stage and then started to decrease after reaching a maximum (Figure 2a). At the maximum of the load, the stress calculated based on the load and sample diameter is 320 MPa when the deformation is assumed to be homogeneous. The large decrease in the load may be contributed to the localization of the deformation because the recovered sample showed the localization (~0.54–0.61 mm in diameter). After the elongation stopped, the load relaxed exponentially. During this deformation, the Q_{FSDP} parallel and perpendicular to the tension showed similar changes as the load (Figure 2e). When the load increased in the initial stage, the Q_{FSDP} decreased, and then the decrease rate became small. After the deformation stopped, the Q_{FSDP} increased with load relaxation. The degree of the Q_{FSDP} change parallel to the tension was larger than that perpendicular to the tension. The molecular-scale strains parallel and perpendicular to the tension direction are shown in Figure 3 with the 1:1 line. When the strain is isotropic, it should follow the 1:1 line; however, our data indicate that the strain was anisotropic (Figure 3). These observations are consistent with those reported in a
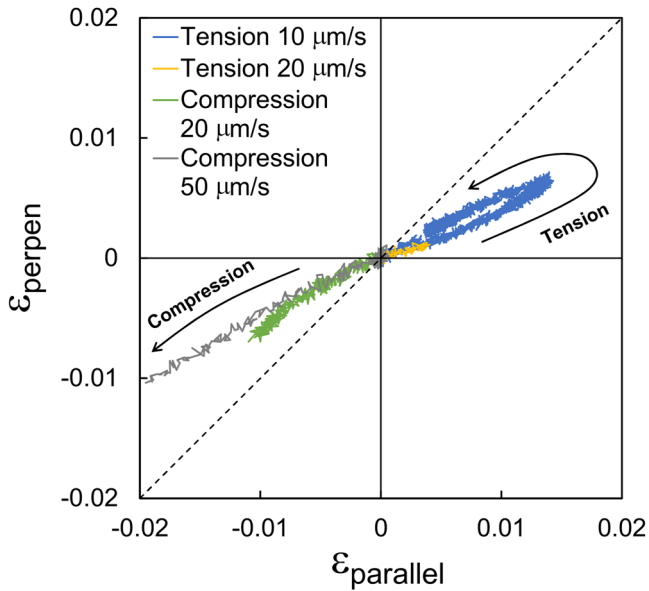
Figure 3. The relationship between molecular-scale strains parallel and perpendicular to tension and compression, represented by $\varepsilon_{parallel}$ and ε_{perpen}, respectively. The molecular-scale strain is defined as $(Q_{FSDP,i} - Q_{FSDP})/Q_{FSDP}$, where $Q_{FSDP,i}$ represents Q_{FSDP} just before deformation (Stoica et al., 2008). The black arrows indicate the direction of the change during tension and compression.

previous study (Okumura et al., 2023). The T–O and T–T distances show did not change under tension (Figure 2i).

In contrast, the sample failed at a rate of 20 μm s⁻¹, resulting in a rapid decrease in the load (Figure 2b). The maximum load corresponds to the stress of 210 MPa. The failure stress of rhyodacite melt under tension is estimated to be ~200–400 MPa when we combine these data with previous data by Okumura et al. (2023), that is, failure at 410 MPa under 10 μm s⁻¹ but the maximum stress of 240 MPa under the elongation without failure at 5 μm s⁻¹. The Q_{FSDP} decreased with increasing load, similar to the changes observed at 10 μm s⁻¹ (Figure 2f). No clear changes were found in the T–O and T–T distances (Figure 2j).

The Q_{FSDP} is related to the intermediate-range ordering of the network with a periodicity of $2\pi/Q_{FSDP}$ (Inamura et al., 1998, 2004; Mei et al., 2008; Wang et al., 2014). Therefore, our observation that Q_{FSDP} decreased with an increase in the load implies that the molecular-scale structure dilated with tension, which may correspond to an increase in the average size of the rings formed by SiO_4 tetrahedra (e.g., Shi et al., 2019; Zhou et al., 2021). Additionally, the dilation was anisotropic because the degree of change in the Q_{FSDP} parallel to the tension was larger than that perpendicular to the tension. In contrast, the T–O and T–T distances did not change under tension. This result indicates that the SiO_4 tetrahedra did not deform and that the T–O–T angle did not change during tension. This result is similar to that predicted from a molecular dynamics simulation of the tension deformation of silicate glass (Bamer et al., 2019).

3.2. Compression Experiments

To clarify the direction of deformation compared to tension, the load in compression is indicated by a negative value. When the compression rate was 20 μm s⁻¹, the degree of the load gradually increased and then started to decrease after reaching a peak, corresponding to the stress of 320 MPa (Figure 2c). The decrease in the load after the peak seems to be due to the onset of the buckling deformation because the load does not show a rapid decrease, which is observed at sample failure. The small decrease during loading may be a local failure or buckling deformation.

At a compression rate of 50 μm s⁻¹, the load increased and then decreased rapidly (Figure 2d), resulting in a sample failure into small fragments. The stress at the failure is 690 MPa. During compression, the Q_{FSDP} values parallel and perpendicular to the compression direction increased continuously, which is opposite to the behavior observed during tension (Figures 2g and 2h). The degree of Q_{FSDP} change parallel to the tension was larger than that perpendicular to tension, indicating that the molecular-scale strain by compression was anisotropic, as observed during tension (Figure 3). The T–O and T–T distances did not show any significant changes during compression (Figures 2k and 2l).

Our observation that Q_{FSDP} increased with increasing compression suggests that molecular-scale structure shrank with compression, probably corresponding to a decrease in the average size of the rings formed by SiO_4 tetrahedra. This result differs from the observations during tension deformation. The T–O and T–T distances did not show any significant changes during compression, indicating that the SiO_4 tetrahedron and T–O–T angle did not deform significantly.

4. Discussions and Conclusions

Our experiments have shown that the molecular-scale structure of silicate melt exhibits elastic and anisotropic dilation during tension and shrinkage during compression (Figure 3) when the deformation rate is slightly lower than the failure criterion, that is, shear thinning condition, or large enough to cause failure. While the deformation style at the molecular level differs between dilation and shrinkage, shear thinning and failure are observed under both tension and compression (e.g., Simmons et al., 1982; Wadsworth et al., 2018; Webb & Dingwell, 1990a, 1990b).

As discussed in previous studies (e.g., Bamer et al., 2019; Okumura et al., 2023), molecular-scale elastic and anisotropic dilation occurs under tension, which is expected to be the origin of shear thinning and brittle failure. In contrast, molecular-scale shrinkage was observed under compression. Molecular dynamics simulations of SiO_2 glass have shown that three- and four-membered rings are energetically unfavorable and unstable compared to five- and six-membered rings that make up most of the silicate structure (e.g., Rino et al., 1993). Moreover, small rings in sodium silicate glass are mechanically robust and can withstand large internal stresses (Song et al., 2019). Shi et al. (2022) proposed that the presence of these strong but unstable small rings in silicate glass and super-cooled melts may be the origin of their fragility. Therefore, when the deformation fluctuates in the sample under compression, the local structural relaxation and viscous reduction could be driven by the change in the ring sizes from unstable small rings to stable large rings, resulting in the localization of deformation and finally shear thinning and failure of a bulk sample.

In our experiments, no clear changes were observed in the T–O and T–T distances, although the intermediate-range ordering varied. This implies that there was no change in the T–O–T angle. Song et al. (2019) indicated that the T–O–T angles in four- and five-membered rings are not different from those in six-membered rings, but the internal stress that can be supported is greatest in four-membered rings and lowest in six-membered rings. In conclusion, a small change in ring size under compression causes viscosity reduction, which could be the origin of shear thinning.

Failure under compression also originates from the large internal stress supported by the strong small rings. Under tension, the fibrous sample failed into two or more pieces, whereas the sample was crushed into many fragments under compression. We could not precisely determine the compressive strength because of the buckling of the sample; however, the failure occurred when the stress was 690 MPa under compression (Figure 2d), which was much larger than the tensile strength (∼200–400 MPa).

Our experiments have revealed that the silicate melts undergo different types of structural changes at the molecular scale under tension and compression, namely dilation and shrinkage. Both types of deformation lead to changes in the intermediate-range ordering of the silicate melt, while no clear changes were observed in the short-range ordering. These results suggest that the non-Newtonian behavior of silicate melts mainly originates from the evolution of intermediate-range ordering during deformation.

The magma failure criterion is often described by comparing the timescale of the Maxwell structural relaxation with the deformation rate, that is, strain rate condition (e.g., Cordonnier et al., 2012; Gonnermann & Manga, 2003; Papale, 1999; Wadsworth et al., 2018). However, this criterion only serves as a "necessary condition" for failure. Under low stress, viscous relaxation is fast, and no elastic deformation occurs in the molecular-scale structure. When the stress is high and the deformation timescale approaches the Maxwell relaxation timescale, elastic and anisotropic deformation of the molecular-scale structure begins, leading to a reduction in viscosity. Under larger stress, the degree of elastic deformation increases, and failure occurs when the stress reaches the strength of the silicate melt. Our experiments demonstrated that the magma does not fail, even at high deformation rate, as long as the stress is low (Figures 2b and 2d). Therefore, we infer that a "necessary and sufficient condition" for magma failure could be described as a stress condition (Zhang, 1999). In nature, gas bubbles and crystals in magma induce stress localization, enhancing the failure of the magma (e.g., Kameda et al., 2017; Zhang, 1999).

Conflict of Interest

The authors declare no conflicts of interest relevant to this study.

Data Availability Statement

All the datasets obtained and discussed in this study are available at https://doi.org/10.5281/zenodo.8133116.

References

Bamer, F., Ebrahem, F., & Markert, B. (2019). Plasticity in vitreous silica induced by cyclic tension considering rate-dependence: Role of the network topology. *Journal of Non-Crystalline Solids*, *503–504*, 176–181. https://doi.org/10.1016/j.jnoncrysol.2018.09.043

Boccato, S., Garino, Y., Morard, G., Zhao, B., Xu, F., Sanloup, C., et al. (2022). Amorpheus: A Python-based software for the treatment of X-ray scattering data of amorphous and liquid systems. *High Pressure Research*, *42*(1), 69–93. https://doi.org/10.1080/08957959.2022.2032032

Caricchi, L., Burlini, L., Ulmer, P., Gerya, T., Vassalli, M., & Papale, P. (2007). Non-Newtonian rheology of crystal-bearing magmas and implications for magma ascent dynamics. *Earth and Planetary Science Letters*, *264*(3–4), 402–419. https://doi.org/10.1016/j.epsl.2007.09.032

Champallier, R., Bystricky, M., & Arbaret, L. (2008). Experimental investigation of magma rheology at 300 MPa: From pure hydrous melt to 76 vol.% of crystals. *Earth and Planetary Science Letters*, *267*(3–4), 571–583. https://doi.org/10.1016/j.epsl.2007.11.065

Chen, Y.-C., Lu, Z., Nomura, K., Wang, W., Kalia, R. K., Nakano, A., & Vashishta, P. (2007). Interaction of voids and nanoductility in silica glass. *Physical Review Letters*, *99*(15), 155506. https://doi.org/10.1103/PhysRevLett.99.155506

Cordonnier, B., Schmalholz, S. M., Hess, K.-U., & Dingwell, D. B. (2012). Viscous heating in silicate melts: An experimental and numerical comparison. *Journal of Geophysical Research*, *117*(B2), B02203. https://doi.org/10.1029/2010JB007982

Di Genova, D., Brooker, R. A., Mader, H. M., Drewitt, J. W. E., Longo, A., Deubener, J., et al. (2020). In situ observation of nanolite growth in volcanic melt: A driving force for explosive eruptions. *Science Advances*, *6*(39), eabb0413. https://doi.org/10.1126/sciadv.abb041

Gonnermann, H. M., & Manga, M. (2003). Explosive volcanism may not be an inevitable consequence of magma fragmentation. *Nature*, *426*(6965), 432–435. https://doi.org/10.1038/nature02138

Goto, A. (1999). A new model for volcanic earthquake at Unzen Volcano: Melt rupture model. *Geophysical Research Letters*, *26*(16), 2541–2544. https://doi.org/10.1029/1999gl900569

Guan, P., Lu, S., Spector, M. J. B., Valavala, P. K., & Falk, M. L. (2013). Cavitation in amorphous solids. *Physical Review Letters*, *110*(18), 185502. https://doi.org/10.1103/PhysRevLett.110.185502

Hess, K.-U., Cordonnier, B., Lavallée, Y., & Dingwell, D. B. (2007). High-load, high-temperature deformation apparatus for synthetic and natural silicate melts. *Review of Scientific Instruments*, *78*(7), 075102. https://doi.org/10.1063/1.2751398

Hess, K.-U., Cordonnier, B., Lavallée, Y., & Dingwell, D. B. (2008). Viscous heating in rhyolite: An in situ experimental determination. *Earth and Planetary Science Letters*, *275*(1–2), 121–126. https://doi.org/10.1016/j.epsl.2008.08.014

Inamura, Y., Arai, M., Kitamura, N., Bennington, S. M., & Hannon, A. C. (1998). Intermediate-range structure and low-energy dynamics of densified SiO_2 glass. *Physica B*, *241–243*, 903–905. https://doi.org/10.1016/s0921-4526(97)00748-5

Inamura, Y., Katayama, Y., Utsumi, W., & Funakoshi, K. (2004). Transformations in the intermediate-range structure of SiO_2 glass under high pressure and temperature. *Physical Review Letters*, *93*(1), 015501. https://doi.org/10.1103/PhysRevLett.93.015501

Kameda, M., Ichihara, M., Maruyama, S., Kurokawa, N., Aoki, Y., Okumura, S., & Uesugi, K. (2017). Advancement of magma fragmentation by inhomogeneous bubble distribution. *Scientific Reports*, *7*(1), 16755. https://doi.org/10.1038/s41598-017-16941-x

Kozono, T., & Koyaguchi, T. (2012). Effects of gas escape and crystallization on the complexity of conduit flow dynamics during lava dome eruptions. *Journal of Geophysical Research*, *117*(B8), B08204. https://doi.org/10.1029/2012JB009343

Kozono, T., & Okumura, S. (2022). Constraints on magma properties at fragmentation during the 2011 sub-Plinian eruptions of Kirishima Shinmoe-dake volcano, Japan. *Journal of Geophysical Research: Solid Earth*, *127*(12), e2022JB025183. https://doi.org/10.1029/2022JB025183

Lange, R. A., & Carmichael, I. S. E. (1990). Thermodynamic properties of silicate liquids with emphasis on density, thermal expansion and compressibility, modern methods of igneous petrology: Understanding magmatic processes. In J. Nicholls & J. K. Russell (Eds.), *Reviews in mineralogy* (Vol. 24, pp. 25–64). Mineralogical Society of America.

Mei, Q., Benmore, C. J., Sen, S., Sharma, R., & Yarger, J. L. (2008). Intermediate range order in vitreous silica from a partial structure factor analysis. *Physical Review B*, *78*(14), 144204. https://doi.org/10.1103/PhysRevB.78.144204

Muralidharan, K., Torras, J., & Trickey, S. B. (2007). Energetics and mechanical properties of silica nanotubes. *Journal of Physics: Condensed Matter*, *19*(38), 386238. https://doi.org/10.1088/0953-8984/19/38/386238

Okumura, S., Kushnir, A. R. L., Martel, C., Champallier, R., Thibault, Q., & Takeuchi, S. (2016). Rheology of crystal-bearing natural magmas: Torsional deformation experiments at 800°C and 100 MPa. *Journal of Volcanology and Geothermal Research*, *328*, 237–246. https://doi.org/10.1016/j.jvolgeores.2016.11.009

Okumura, S., Uesugi, K., Goto, A., Namiki, A., Matsumoto, K., & Sakamaki, T. (2023). Molecular-scale structural changes of silicate melts under tension revealed by time-resolved X-ray diffraction. *Chemical Geology*, *621*, 121372. https://doi.org/10.1016/j.chemgeo.2023.121372

Okumura, S., Uesugi, K., Goto, A., Sakamaki, T., Matsumoto, K., Takeuchi, A., & Miyake, A. (2022). Rheology of nanocrystal-bearing andesite magma and its roles in explosive volcanism. *Communication of Earth and Environment*, *3*(1), 241. https://doi.org/10.1038/s43247-022-00573-9

Okumura, S., Uesugi, K., Sakamaki, T., Goto, A., Uesugi, M., & Takeuchi, A. (2020). An experimental system for time-resolved X-ray diffraction of deforming silicate melt at high temperature. *Review of Scientific Instruments*, *91*(9), 09113. https://doi.org/10.1063/5.0009769

Papale, P. (1999). Strain-induced magma fragmentation in explosive eruptions. *Nature*, *397*(6718), 425–428. https://doi.org/10.1038/17109

Rino, J. P., Ebbsjö, I., Kalia, R. K., Nakano, A., & Vashishta, P. (1993). Structure of rings in vitreous SiO_2. *Physical Review B*, *47*(6), 3053–3062. https://doi.org/10.1103/physrevb.47.3053

Shi, Y., Deng, B., Gulbiten, O., Nauchy, M., Zhou, Q., Neuefeind, J., et al. (2022). Revealing the relationship between liquid fragility and medium-range order in silicate glasses. *Nature Communications*, *14*(1), 13. https://doi.org/10.1038/s41467-022-35711-6

Shi, Y., Neuefeind, J., Ma, D., Page, K., Lamberson, L. A., Smith, N. J., et al. (2019). Ring size distribution in silicate glasses revealed by neutron scattering first sharp diffraction peak analysis. *Journal of Non-Crystalline Solids*, *516*, 71–81. https://doi.org/10.1016/j.jnoncrysol.2019.03.037

Simmons, J. H., Mohr, R. K., & Montrose, C. J. (1982). Non-Newtonian viscous flow in glass. *Journal of Applied Physics*, *53*(6), 4075–4080. https://doi.org/10.1063/1.331272

Song, W., Li, X., Wang, B., Anoop Krishnan, N. M., Goyal, S., Smedskjaer, M. M., et al. (2019). Atomic picture of structural relaxation in silicate glasses. *Applied Physics Letters*, *114*(23), 233703. https://doi.org/10.1063/1.5095529

Stoica, M., Das, J., Bednarcik, J. D., Franz, H., Mattern, N., Wang, W. H., & Eckert, J. (2008). Strain distribution in $Zr_{64.13}Cu_{15.75}Ni_{10.12}Al_{10}$ bulk metallic glass investigated by in situ tensile tests under synchrotron radiation. *Journal of Applied Physics*, *104*(1), 013522. https://doi.org/10.1063/1.2952034

Sun, B. A., & Wang, W. H. (2015). The fracture of bulk metallic glasses. *Progress in Materials Science*, *74*, 211–307. https://doi.org/10.1016/j.pmatsci.2015.05.002

Vasseur, J., Wadsworth, F. B., & Dingwell, D. B. (2023). Shear thinning and brittle failure in crystal-bearing magmas arise from local non-Newtonian effects in the melt. *Earth and Planetary Science Letters*, *603*, 117988. https://doi.org/10.1016/j.epsl.2023.117988

Wadsworth, F. B., Witcher, T., Vossen, C. E. J., Hess, K.-U., Unwin, H. E., Scheu, B., et al. (2018). Combined effusive-explosive silicic volcanism straddles the multiphase viscous-to-brittle transition. *Nature Communications*, *9*(1), 4696. https://doi.org/10.1038/s41467-018-07187-w

Wang, Y., Sakamaki, T., Skinner, L. B., Jing, Z., Yu, T., Kono, Y., et al. (2014). Atomistic insight into viscosity and density of silicate melts under pressure. *Nature Communications*, *5*(1), 3241. https://doi.org/10.1038/ncomms4241

Webb, S. L., & Dingwell, D. B. (1990a). Non-Newtonian rheology of igneous melts at high stresses and strain rates: Experimental results for rhyolite, andesite, basalt, and nephelinite. *Journal of Geophysical Research*, *95*(B10), 15695–15701. https://doi.org/10.1029/jb095ib10p15695

Webb, S. L., & Dingwell, D. B. (1990b). The onset of non-Newtonian rheology of silicate melts. *Physics and Chemistry of Minerals*, *17*(2), 125–132. https://doi.org/10.1007/bf00199663

Williams, Q., & Jeanloz, R. (1988). Spectroscopic evidence for pressure-induced coordination changes in silicate glasses and melts. *Science*, *239*(4842), 902–905. https://doi.org/10.1126/science.239.4842.902

Wilson, L., Sparks, R. S. J., & Walker, G. P. L. (1980). Explosive volcanic eruptions—IV. The control of magma properties and conduit geometry on eruption column behaviour. *Geophysical Journal International*, *63*(1), 117–148. https://doi.org/10.1111/j.1365-246x.1980.tb02613.x

Yuan, F., & Huang, L. (2014). Brittle to ductile transition in densified silica glass. *Scientific Reports*, *4*(1), 5035. https://doi.org/10.1038/srep05035

Zhang, Y. (1999). A criterion for the fragmentation of bubbly magma based on brittle failure theory. *Nature*, *402*(6762), 648–650. https://doi.org/10.1038/45210

Zhou, Q., Shi, Y., Deng, B., Neuefeind, J., & Bauchy, M. (2021). Experimental method to quantify the ring size distribution in silicate glasses and simulation validation thereof. *Science Advances*, *7*(28), eabh1761. https://doi.org/10.1126/sciadv.abh1761